ELSEVIER

Short-lived magmatic activity in an anorogenic subvolcanic complex: $^{40}Ar/^{39}Ar$ and ion microprobe U–Pb zircon dating of the Erongo, Damaraland, Namibia

Marcus Wigand [a,*], Axel K. Schmitt [a], Robert B. Trumbull [a], Igor M. Villa [b], Rolf Emmermann [a,c]

[a] *GeoForschungsZentrum Potsdam, Telegrafenberg, 14473 Potsdam, Germany*
[b] *Gruppe Isotopengeologie, Universität Bern, 3012 Bern, Switzerland*
[c] *Institut für Geowissenschaften und Lithosphärenforschung, Universität Giessen, Am Zeughaus 1, 35390 Giessen, Germany*

Abstract

The Erongo subvolcanic center in Namibia is the largest composite, bimodal complex in the Mesozoic Etendeka igneous province of Namibia. This study of $^{40}Ar/^{39}Ar$ and high spatial resolution U–Pb zircon dating demonstrates that emplacement of the various igneous units at Erongo took place within a time span equivalent to or shorter than geochronologically resolvable age differences (ca. 2 Ma), and at the peak of regional flood-basalt activity in the Etendeka–Paraná province. The Erongo complex comprises a series of felsic volcanic and intrusive units that overlie or intrude basaltic lavas attributed to the Etendeka Group. The stratigraphically oldest rhyodacite (Erongorus unit) yielded U–Pb zircon ages of 131.8 ± 1.1 Ma (1σ). The overlying Ombu rhyodacite was previously dated at 135.0 ± 1.6 Ma and our new ages for a resurgent intrusion of the same magma type (Ombu granodiorite) in the vent area are 132.6 ± 1.1 Ma ($^{40}Ar/^{39}Ar$) and 132.3 ± 1.9 Ma (U–Pb zircon) respectively. The youngest felsic magmas at Erongo are the high-silica Ekuta rhyolite and compositionally equivalent Erongo granite. These units yielded U–Pb zircon ages of 131.9 ± 2.9 and 130.3 ± 1.4 Ma, respectively. Concordant $^{40}Ar/^{39}Ar$ biotite ages from two samples of the granite average 132.2 ± 0.8 Ma. The final stage of magmatism at Erongo involved emplacement of basic alkaline plugs and dikes. Phlogopite and kaersutite from foidite plugs of this series yielded $^{40}Ar/^{39}Ar$ ages of 130.8 ± 1.0 and 132.0 ± 1.0 Ma. In a regional context, these age results indicate that silicic magmatism in the largest complexes of the Damaraland (Erongo, Brandberg, Paresis, Messum) began simultaneously with the peak of flood-basalt effusion at about 132 Ma throughout the Etendeka province and ceased by about 130 Ma. The silicic magmas are hybrid, with varying contributions of crustal and mantle-derived melts, and the age constraints suggest that crustal melting was caused by a short-lived thermal pulse related to the main flood-basalt event. Basic magmatism in the Damaraland complexes continued sporadically thereafter to about 123 Ma, but lacked the power to create further crustal melting.
© 2003 Elsevier B.V. All rights reserved.

Keywords: Ar/Ar; U/Pb; Paraná–Etendeka; anorogenic granite; flood basalt; silicic magmatism

---

* Corresponding author. Tel.: +49-331-288-1468; Fax: +49-331-288-1474.
  E-mail address: wigand@gfz-potsdam.de (M. Wigand).

1. Introduction

Precise estimates of the onset and duration of silicic volcanism in continental large igneous provinces are important parameters not only for constraining the age relations with intercalated basaltic flows but also for insights into the broader questions of mantle dynamics and melt generation within thinned continental crust during rift-ing and continental break-up (Kirstein et al., 2001; Bryan et al., 2002). The Etendeka–Paraná is a prominent example of a bimodal igneous province, where flood basalts are intercalated with silicic lavas and ignimbrite sheets. While there is consensus that volcanism occurred during break-up of western Gondwanaland prior to opening of the South Atlantic (e.g. Erlank et al., 1984; Milner et al., 1995; Renne et al., 1996), its
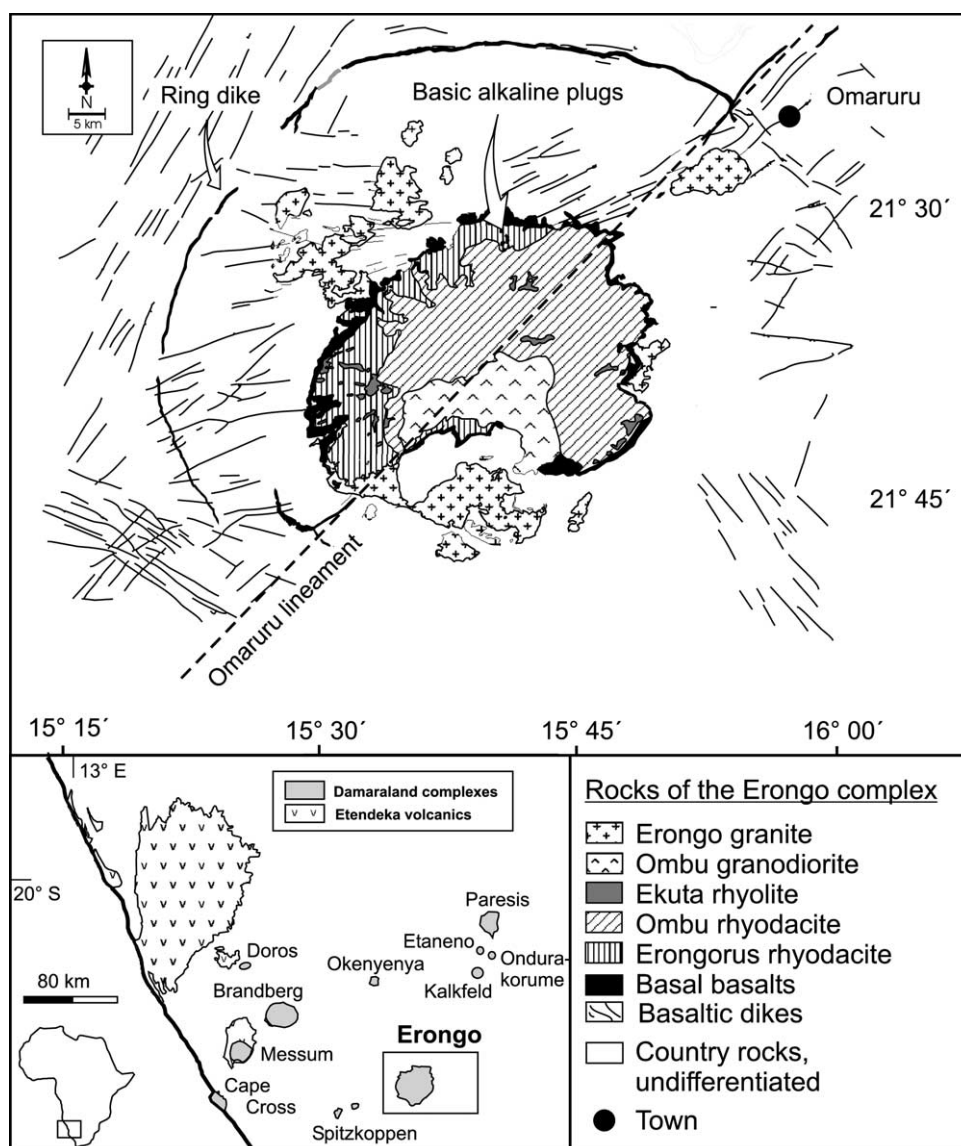

Fig. 1. Simplified geologic map of the Erongo complex modified from Milner (1997). The inset shows the position of the Erongo among the other Damaraland subvolcanic complexes and the distribution of Etendeka Group volcanic rocks in NW Namibia.

duration has been controversially discussed (e.g. Renne et al., 1992; Stewart et al., 1996; Peate, 1997). For example, Marsh et al. (2001) compiled stratigraphic sections through basaltic and silicic units in the Etendeka province and suggested emplacement of the entire sequence at 132 ± 1 Ma whereas Kirstein et al. (2001) described protracted felsic volcanism from the conjugate margin in southern Uruguay that extends as much as 5 Ma younger than the Etendeka units. Part of the controversy on the duration of Etendeka–Paraná volcanism may result from comparing results from different regional foci (Peate, 1997). Kirstein et al. (2001) further discussed technical problems including the interlaboratory comparability of $^{40}Ar/^{39}Ar$ results. In addition, there is an ongoing controversy regarding the K–Ar age and uncertainties of reference minerals used for monitoring neutron flux (Renne et al., 1998).

Previous dating studies of the regionally extensive silicic volcanic units in the Etendeka–Paraná province (e.g. Milner et al., 1995; Kirstein et al., 2001) have the disadvantage that the eruptive sites are rarely known and, consequently, it is difficult to link the age data with information on the magma evolution of individual systems (Marsh et al., 2001). An important additional focus for study are the silicic subvolcanic stocks or anorogenic granite intrusions that are well exposed in the Damaraland area south of the main Etendeka lava field (Fig. 1). The Damaraland complexes (e.g. Martin et al., 1960; Harris, 1995; Trumbull et al., 2000) comprise about 20 intrusions and dike swarms with a great variety of rock types including both silica-undersaturated series (carbonatite, basic alkaline–syenite–foyaite associations) and oversaturated series (tholeiitic gabbro–granodiorite–granite and volcanic equivalents). Monolithologic intrusions are rare and small in size, whereas all of the larger complexes are composite, with an internal variation that in some cases spans much of the compositional range displayed in the Damaraland complexes as a whole. Petrogenetic studies of the composite complexes are well advanced and have concluded that extensive differentiation of mantle-derived magmas and partial melting of the crust with subsequent magma mixing combined to produce the lithologic

variations (i.e. *Messum*: Harris et al., 1999; Ewart et al., 2002; *Okenyenya*: Martinez et al., 1996; Milner and Le Roex, 1996; *Paresis*, Mingram et al., 2000; *Brandberg*, Schmitt et al., 2000; *Erongo*, Pirajno, 1990; authors' unpublished data). However, the time span over which these processes occurred is poorly constrained. K/Ar and Rb/Sr age data of the Messum and Okenyenya complex suggest that some of these composite complexes were assembled over considerable time spans, as long as 5–10 Ma (Milner et al., 1995; Peate, 1997). Field relations indicate that the intrusive complexes post-date regional Etendeka flood volcanism but it is unclear from present geochronologic data how large the gap may be. For the Brandberg complex, Schmitt et al. (2000) demonstrated from $^{40}Ar/^{39}Ar$ ages of biotite, hornblende and astrophyllite that the evolution of metaluminous granite to highly evolved and mineralized peralkaline granites took place within a short range of $\sim$132–131 Ma, which is indistinguishable from the age span of Etendeka basalts and felsic volcanic rocks from Namibia (Marsh et al., 2001).

In this study we focus on the duration of igneous activity at the composite Erongo complex based on new $^{40}Ar/^{39}Ar$ and high-spatial-resolution U–Pb zircon ages from the main units, with emphasis on the silicic magmatism. Erongo is the largest among the Damaraland complexes and also one of the compositionally most distinct because of the close association of peraluminous, crustal-derived silicic volcanic rocks and granites (Harris, 1995; Trumbull et al., 2000) with mantle-derived tholeiitic and alkaline basaltic rocks (Trumbull et al., 2003). The few existing age determinations of the Erongo complex have given ambiguous results. Samples of granite yielded a whole-rock Rb–Sr isochron age of 144 ± 2 Ma (McNeill, 1989), which conflicts with the geologic observation that sills of this granite intrude a rhyodacite tuff unit from which a SHRIMP U–Pb zircon age of 135 ± 1.6 Ma (1σ) was reported by Pirajno et al. (2000). Erongo is also important for stratigraphic correlation of regional flood volcanism because volcanic units at its base are suggested to represent distal deposits of the Etendeka regional volcanic sequence (Emmermann, 1979;

Pirajno, 1990, Pirajno et al., 2002), the closest confirmed outcrops of which are located more than 100 km to the NW (Fig. 1).

The new ages presented here document a short duration for silicic magmatic activity at Erongo, an age equivalence with other large composite intrusions of the Damarland complexes, and an overlap with the peak age of flood basalts from the Etendeka Group. A picture is emerging that large-scale basaltic underplating followed by crustal melting, ascent, differentiation, and eruption of the silicic magmas took place throughout the Etendeka province within a time span of about 2 million years at most.

2. Geological setting

The Erongo complex is the largest of the Damaraland complexes and has been the subject of several geologic and geochemical studies (Cloos, 1911, 1919; Emmermann, 1979; Pirajno, 1990; Pirajno et al., 2000; Trumbull et al., 2003; authors' unpublished data). The complex consists of three main morpho-structural units: (1) a cen-

tral massif about 30 km in diameter and made up principally of volcanic units; (2) peripheral granite intrusions dispersed around the central massif; and (3) a prominent semi-circular ring dike of tholeiitic dolerite some 50 km in diameter (Fig. 1). The Erongo complex was emplaced along the Omaruru lineament, which was established in the Neoproterozoic Damara orogeny and constitutes the boundary between two litho-tectonic zones of the Damara belt (Miller, 1983). The country rocks are Neoproterozoic metasediments (Kuiseb pelitic schists and metagreywacke) of the Damara sequence and post-tectonic S-type Damara granites of Early Cambrian age (Miller, 1983). These rocks are locally overlain by Mesozoic fluvial sediments of the Krantzberg and Lionshead formations, which are dominated by locally derived detritus of the Damara sequence and whose irregular outcrop distribution and variable thickness suggest deposition in local basins, perhaps related to Mesozoic faulting (Hegenberger, 1988). Indeed, Mesozoic reactivation of the Omaruru lineament is documented by overthrusting of Karoo sedimentary rocks over the Damara sequence along the Waterberg fault NE of Erongo. The lineament
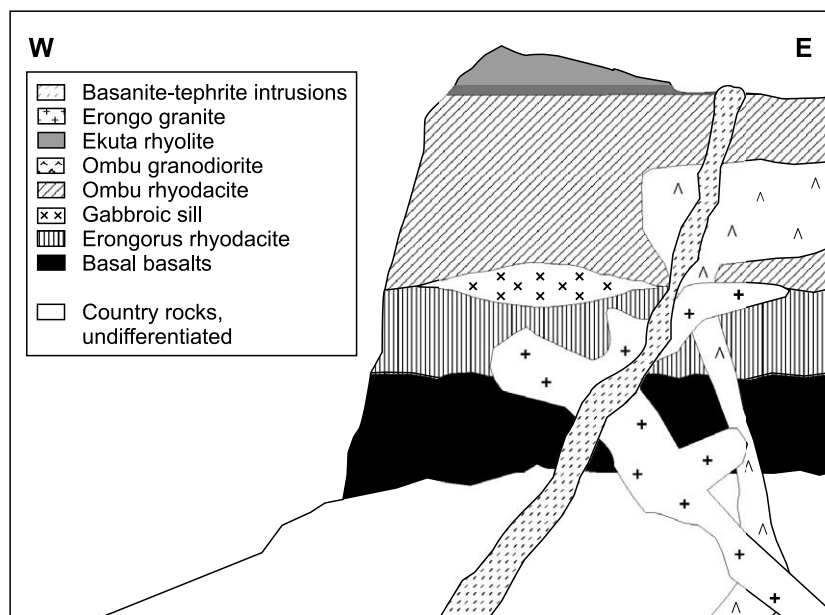

Fig. 2. Schematic stratigraphic and intrusive section of the Erongo complex based on exposures on the western margin and on profiles by Pirajno (1990).

apparently was also active during and after emplacement of the Erongo complex because it limits the extent of the ring dike and there is a marked asymmetry of units within the central massif on either side (see below). A minor offset of Erongo units across the lineament is present at the NE margin of the complex and several felsic dikes have filled fractures along the lineament zone (T. Vietor, personal communication, 2003).

The stratigraphy and contact relations in the central Erongo massif suggest the following sequence of magmatic units (Fig. 2). Nomenclature of the units follows that in the 1:250 000 geologic map of Namibia (Milner, 1997).

(1) Basal tholeiitic basalts were erupted over the Damara sequence or, depending on the paleotopography, on Triassic sedimentary rocks. Pirajno et al. (2000) suggested that these lavas were fed from nearby basic dikes including the semi-circular ring dike (which they termed a cone sheet). A detailed geochemical study of the basal basalts (authors' unpublished data) confirms their compositional similarity with the Tafelberg basalts of the Etendeka Group, but shows that the ring-dike dolerite is compositionally distinct and belongs to the Erongo magmatic event. We suggest that the ring dike formed after caldera collapse of the central massif following eruption of the main silicic magmas. This is supported by the presence of a gabbro sill within the silicic tuffs which is compositionally identical to the ring dike (authors' unpublished data).

(2) Two distinct series of silicic lavas and tuffs overlie the basal basalts: the lower Erongorus and the upper Ombu rhyodacite (Fig. 2). The two units are compositionally similar but the Ombu rhyodacite is easily distinguished by the abundance of coarse lithic fragments of Damara granite and schist, and by the presence of vitrophyre horizons. The lithic-free Erongorus rhyodacite is unevenly distributed, being present only along the NW margin of the complex, where it reaches a maximal thickness of 370 m. On the north, east and southern margins of the complex, the Ombu rhyodacite directly overlies basalt. This suggests pre-eruptive topography perhaps related to reactivation of the Omaruru lineament. The Ombu

rhyodacite, with thicknesses typically in excess of 500 m, is the most voluminous unit of the Erongo complex and its eruption is thought to be the main caldera-forming event (Pirajno, 1990). A subvolcanic equivalent of the rhyodacite is exposed in the low, central portion of the complex. This unit, the Ombu granodiorite, shows the same distinctive assemblage of lithic fragments and a gradational contact with the overlying rhyodacite (Emmermann, 1979). The topographic depression occupied by the Ombu granodiorite is interpreted as the vent region for the Ombu eruption (Pirajno, 1990). In addition to the central Ombu granodiorite there are several dikes of similar composition and coarse-grained texture that occur outside the main massif to the east.

(3) A final silicic volcanic unit, the Ekuta rhyolite, is preserved in scattered erosional remnants at higher elevations in the central massif where it overlies Ombu rhyodacite. The rhyolite has a finely laminated texture and the presence of fiamme and locally derived rip-up clasts suggests that the unit originated as an ash-flow tuff. It lacks the lithic fragments that are so characteristic of the underlying Ombu unit. Mineralogically and chemically, the Etuka rhyolite resembles the Erongo granite.

(4) The Erongo granite forms a series of stocks intruded into Damara rocks outside the central massif (Fig. 1) and it also occurs in sills and dikes that cut the Ombu rhyodacite. The granite is a homogeneous tourmaline-bearing biotite granite which is characterized by the presence of rounded tourmaline–quartz segregations. Intrusion of the Erongo granite and/or the eruption of the Ekuta rhyolite with which it may be genetically related marks the final stage of silicic magmatism at Erongo.

(5) The last phase of igneous activity at Erongo involves basic alkaline magmas. Ombu rhyodacites in the central massif are cut by basic alkaline dikes and small basanite–tephro–phonolite intrusions (for simplicity named foidites; Trumbull et al., 2003) and the Erongo granite on Anibib farm NW of the complex is cut by alkaline basaltic dikes. The latter show flexures, indicating that the granite was not fully solidified at the time of dike intrusion (Emmermann, 1979).

Table 1
Ar–Ar stepwise heating results

Step	T (°C)	$^{40}Ar_{tot}$[a]	$^{40}Ar_{tot}$[a] 1σ	^{39}Ar[a]	^{39}Ar[a] 1σ	^{38}Ar[a]	^{38}Ar[a] 1σ	^{37}Ar[a]	^{37}Ar[a] 1σ	^{36}Ar[a]	^{36}Ar[a] 1σ	Age (Ma)	± Age (Ma) 1σ
Sample 432													
1	573	32.88	0.27	0.287	0.003	0.050	0.003	0.088	0.002	0.031	0.003	78.0	2.9
2	700	479.03	0.03	3.223	0.003	0.178	0.001	0.004	0.006	0.078	0.001	130.7	0.2
3	780	385.01	0.06	2.593	0.003	0.131	0.001	–	–	0.063	0.002	130.5	0.3
4	827	301.48	0.02	1.966	0.003	0.097	0.002	0.054	0.002	0.075	0.002	131.2	0.3
5	873	103.81	0.02	0.627	0.002	0.045	0.002	0.056	0.002	0.049	0.001	131.4	0.7
6	917	77.43	0.01	0.424	0.002	0.050	0.001	–	–	0.057	0.002	131.8	1.4
7	990	30.76	0.01	0.167	0.001	0.020	0.001	0.033	0.007	0.050	0.002	89.0	3.3
8	1021	134.44	0.03	0.731	0.002	0.069	0.001	0.066	0.002	0.102	0.002	131.8	0.9
9	1188	110.81	0.08	0.599	0.002	0.033	0.001	0.091	0.007	0.084	0.002	132.5	1.1
10	1427	25.02	0.01	0.061	0.001	0.014	0.001	0.020	0.002	0.056	0.001	126.6	9.4
Sample 435													
1	629	7.20	0.02	0.035	0.002	0.061	0.002	–	–	0.017	0.002	60.5	20.2
2	894	35.30	0.01	0.165	0.002	0.255	0.002	0.227	0.007	0.037	0.002	136.4	3.9
3	979	160.89	0.03	1.048	0.002	0.231	0.003	3.447	0.013	0.049	0.002	129.0	0.5
4	1006	315.39	0.03	2.108	0.004	0.368	0.002	7.131	0.024	0.045	0.002	132.2	0.3
5	1037	220.16	0.02	1.487	0.003	0.254	0.002	4.958	0.017	0.027	0.002	131.6	0.4
6	1064	45.31	0.01	0.273	0.002	0.062	0.002	0.947	0.008	0.023	0.002	129.8	2.2
7	1086	25.75	0.01	0.143	0.003	0.035	0.002	0.479	0.009	0.010	0.002	146.0	4.2
8	1188	35.56	0.01	0.211	0.002	0.047	0.001	0.797	0.009	0.017	0.002	133.2	2.3
9	1429	149.83	0.02	0.975	0.003	0.227	0.001	3.566	0.014	0.040	0.001	130.7	0.5
Sample 391													
1	581	23.38	0.39	0.292	0.008	0.076	0.004	0.035	0.006	0.058	0.003	19.9	4.0
2	698	27.16	0.21	0.273	0.005	0.056	0.002	0.026	0.003	0.059	0.002	33.2	2.9
3	778	38.28	0.07	0.209	0.001	0.060	0.002	–	–	0.071	0.002	77.1	2.3
4	826	20.62	0.01	0.111	0.001	0.011	0.001	–	–	0.014	0.002	136.0	5.5
5	857	35.34	0.01	0.193	0.002	0.014	0.002	0.004	0.003	0.023	0.001	135.8	2.4
6	901	1961.63	0.40	13.189	0.013	0.763	0.001	0.108	0.002	0.187	0.002	132.5	0.1
7	941	626.25	0.17	4.242	0.005	0.253	0.001	0.052	0.001	0.039	0.001	132.8	0.2
8	1024	210.79	0.02	1.380	0.002	0.067	0.001	0.015	0.002	0.016	0.003	136.8	0.5
9	1188	60.06	0.01	0.387	0.003	0.020	0.002	0.006	0.004	0.042	0.001	113.1	1.3
Sample 454													
1	570	21.06	0.39	0.276	0.008	0.091	0.003	–	–	0.041	0.003	30.9	4.1
2	701	30.59	0.07	0.164	0.003	0.056	0.001	0.057	0.002	0.066	0.002	63.2	4.8
3	782	69.14	0.01	0.330	0.002	0.145	0.002	0.064	0.002	0.083	0.002	123.7	1.8
4	828	54.98	0.01	0.287	0.000	0.099	0.001	0.052	0.003	0.041	0.001	136.2	1.3
5	930	738.06	0.05	4.362	0.005	1.780	0.003	0.071	0.005	0.358	0.002	132.4	0.2
6	927	789.50	0.08	5.326	0.006	2.118	0.004	–	–	0.038	0.002	133.4	0.2
7	982	337.24	0.05	2.230	0.003	0.871	0.003	0.002	0.001	0.028	0.002	134.8	0.3
8	1023	23.74	0.01	0.112	0.002	0.028	0.001	–	–	0.019	0.002	146.9	5.4
9	1201	11.57	0.01	0.049	0.002	0.008	0.001	–	–	0.017	0.002	123.0	14.7
10	1428	11.04	0.01	0.012	0.001	0.004	0.002	0.010	0.002	0.032	0.002	126.2	36.7
Sample 212													
1	582	41.82	0.17	0.367	0.011	0.138	0.003	0.023	0.003	0.058	0.002	62.4	3.7
2	708	412.78	0.02	2.579	0.003	1.018	0.002	–	–	0.122	0.001	133.7	0.2
3	784	260.67	0.04	1.711	0.002	0.659	0.002	0.013	0.004	0.041	0.001	133.0	0.2
4	833	213.73	0.01	1.386	0.002	0.554	0.001	–	–	0.041	0.001	133.1	0.3
5	876	333.18	0.08	2.189	0.003	0.872	0.002	–	–	0.041	0.002	134.3	0.2
6	920	490.27	0.06	3.248	0.003	1.266	0.003	0.012	0.006	0.074	0.002	132.0	0.2
7	960	143.22	0.03	0.911	0.001	0.347	0.002	0.007	0.005	0.061	0.001	126.1	0.4
8	1020	39.77	0.05	0.214	0.001	0.077	0.002	0.058	0.004	0.046	0.001	113.2	1.9
9	1199	28.22	0.01	0.092	0.002	0.013	0.003	0.015	0.001	0.049	0.001	137.2	8.5
10	1427	36.22	0.08	0.058	0.001	0.017	0.002	–	–	0.091	0.002	146.5	14.6

–, below detection limit.

[a] All Ar concentrations are in picoliters per gram (pl/g).

3. Samples and analytical methods

Samples selected for dating were chosen from stratigraphically well-constrained units that would bracket the duration of silicic magmatism. Attempts to date the basal basalts from Ar–Ar determinations of plagioclase separates proved unsuccessful due probably to the minor but unavoidable alteration (authors' unpublished data). The $^{40}Ar/^{39}Ar$ dating therefore concentrated on units with K-rich minerals and these include the Erongo granite, Ombu granodiorite and the late-stage basic alkaline intrusions. Samples of the Erongo granite and Ombu granodiorite were also selected for high-spatial-resolution U–Pb zircon dating. An independent dating method is particularly important for the Ombu unit because of the possibility of excess Ar introduced from the abundant crustal xenoliths. Also chosen for zircon dating were the Erongorus rhyodacite and Ekuta rhyolite, whose degree of alteration makes them unsuitable for $^{40}Ar/^{39}Ar$ dating. We chose not to date the Ombu rhyodacite because there is clear lithologic and geologic evidence for its equivalence to the Ombu granodiorite and it was previously dated by the SHRIMP U–Pb zircon method (Pirajno et al., 2000).

3.1. Ar isotope analyses

Mineral separates were prepared from the 125–200 μm size fraction of crushed whole-rock samples using standard heavy-liquid, magnetic separation techniques and hand-picking. To aid in interpretation of Ar isotope results, portions of the separates were embedded in epoxy sample mounts and analyzed with a CAMECA SX 100 electron microprobe at the GeoForschungsZentrum Potsdam. The calibration employed natural and synthetic mineral standards and all analyses were performed at 15 kV accelerating voltage and 20 nA beam current. PAP corrections were made using CAMECA software (Pouchou and Pichoir, 1984).

Samples were irradiated in the research reactor at McMaster University. Variation of neutron flux was monitored using the reference McClure Mountain hornblende MMhb-1 (Samson and Alexander, 1987). Analyses were carried out at

the University of Bern. The argon was liberated by incremental heating in a double-vacuum resistance furnace, and isotope ratios were measured using a MAP™ 215-50B rare gas mass spectrometer equipped with a single Faraday collector. Details of analytical procedures are presented by Villa et al. (2000). The duration of the single heating steps was between 20 and 45 min. The resulting data (Table 1) were corrected for mass spectrometer background (0.5 ± 0.15 fl for masses 36, 37 and 39), mass discrimination (0.13%/amu), furnace blank (atmospheric composition ranging from 0.2 pl (1000°C) to 0.5 pl (1400°C)) and post-irradiation decay of ^{37}Ar. Neutron-induced interference factors ($(^{39}Ar/^{37}Ar)_{Ca} = 0.00067$; $(^{38}Ar/^{37}Ar)_{Ca} = 0.00023$; $(^{36}Ar/^{37}Ar)_{Ca} = 0.000255$; $(^{40}Ar/^{39}Ar)_K = 0.011$; $(^{38}Ar/^{39}Ar)_K = 0.0118$) were also considered in correction of the final results. We adopted the production rates from Ca and Cl calculated by Onstott et al. (1995). Errors in Table 1 are in-run statistics only (assigned uncertainties of 0.35% on mass discrimination and 1.5–3% on interference corrections) and do not include external uncertainties on J gradient, monitor age and decay constants. According to Renne et al. (1998) the combination of the latter sources of uncertainty amounts to about 1.5% (Renne et al., 1998). Errors quoted in the following sections are at the 1σ level and include the analytical and external uncertainties as described.

3.2. U–Pb zircon analyses

Hand-picked zircons were mounted in epoxy, sectioned and polished to expose grain interiors. The mounts were ultrasonically cleaned and the zircon grains were surveyed via cathodoluminescence (CL) imaging using a Leo 1430VP scanning electron microscope. U–Pb ages were obtained using the CAMECA ims 1270 ion probe at UCLA. A ∼15 nA $^{16}O^-$ beam was focused to a ∼30–35 μm diameter spot on the Au-coated grain surface and secondary ions were extracted at 10 kV with an energy band-pass of 35 eV. The masses $^{94}Zr_2^{16}O^+$, $^{204}Pb^+$, $^{206}Pb^+$, $^{207}Pb^+$, $^{208}Pb^+$, $^{238}U^+$, $^{232}Th^{16}O^+$, and $^{238}U^{16}O^+$ were analyzed at a mass resolution of ∼5000, which is sufficient to resolve molecular interferences except hydrides. The sam-

ple chamber was flooded with O_2 at a pressure of $\sim 4 \times 10^{-3}$ Pa to enhance Pb ion intensities. Prior to analysis, surfaces were pre-sputtered for four min to minimize surficial Pb contamination. Ratios of $^{206}Pb/^{204}Pb = 18.9$, $^{207}Pb/^{204}Pb = 15.6$ and $^{208}Pb/^{204}Pb = 38.3$ (Sañudo-Wilhelmy and Flegal, 1994) were used to correct for remaining common Pb, because these values are typical for local anthropogenic Pb that is the main source of sam-

ple contamination. Relative sensitivities for Pb and U were determined on reference zircon AS-3 (1099 Ma; Paces and Miller, 1993) using a calibration technique similar to that of Compston et al. (1984). Th and U abundances were estimated from measured $^{232}Th^{16}O^+/^{94}Zr_2^{16}O^+$ and $^{238}U^{16}O^+/^{94}Zr_2^{16}O^+$ intensity ratios on unknowns compared to those on reference zircon *91500* (Wiedenbeck et al., 1995).
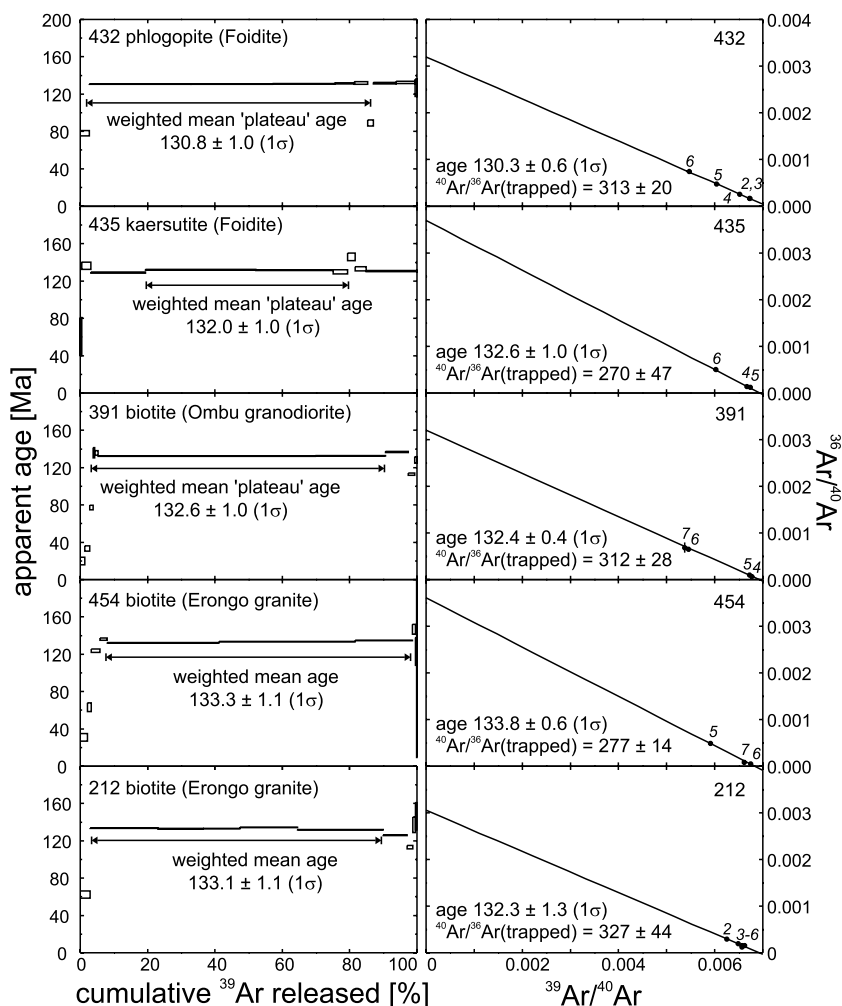

Fig. 3. Age vs. Ar-release spectra for step-heating experiments and corresponding isochron ($^{36}Ar/^{40}Ar$ vs. $^{39}Ar/^{40}Ar$) plots. Steps used for regression are indicated by numbers on the isochrons. Weighted mean (and plateau) ages and regression ages are given for 1σ analytical errors only.

4. Results

4.1. $^{40}Ar/^{39}Ar$ ages

Argon isotope step-heating measurements were made on mineral separates (biotite and amphibole) from the Ombu granodiorite, Erongo gran-ite and foidite plugs. The results are reported in Table 1. For individual samples, we calculated weighted mean ages from 3 to 7 adjacent temperature steps having the same Ca/K and Cl/K signature and from linear regressions through the same steps in a $^{36}Ar/^{40}Ar$ vs. $^{39}Ar/^{40}Ar$ diagram (Fig. 3). All ages reported were calculated using a

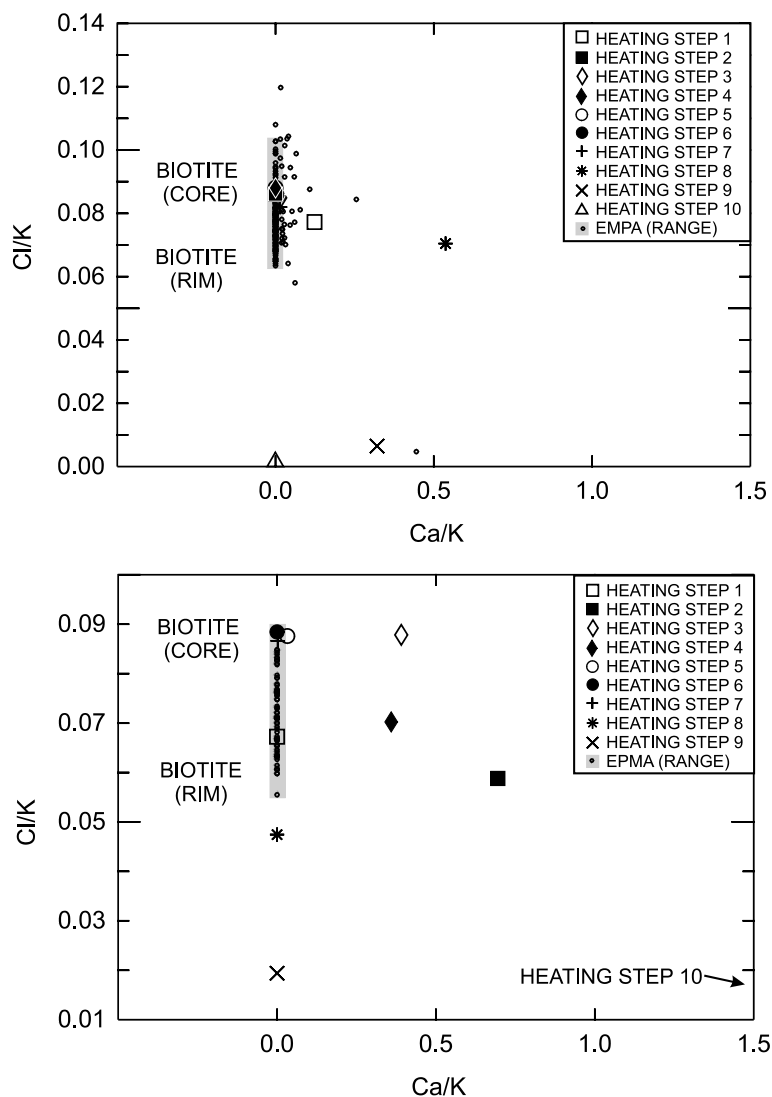Fig. 4. Comparison of Ca/K ($^{37}Ar/^{39}Ar$) and Cl/K ($^{38}Ar/^{39}Ar$) ratios of the step-heating procedure with the Ca/K and Cl/K ratios that were obtained by the electron microprobe analyses (EMPA) of the biotite separates of the Erongo granite (samples 212 and 454). Following the method described by Villa et al. (2000), only intermediate-temperature heating steps were considered for the calculation of the weighted average ages that have equal Ca/K and Cl/K ratios as the biotite. Note that Ca/K ratios of biotite are practically zero, because biotite contains no stoichiometric Ca and that heating steps with Ca/K ratios > 0 were likely influenced by secondary mineralization.

520.4 Ma age of the flux monitor MMhb-1 (Samson and Alexander, 1987) which allows direct comparison with the previously reported ^{40}Ar/^{39}Ar ages from the Etendeka province (e.g. Renne et al., 1996; Schmitt et al., 2000; Pirajno et al., 2000; Kirstein et al., 2001). In calculating the weighted average ages and their uncertainty, errors were scaled by the square root of the mean square of weighted deviates (MSWD) if the MSWD was >1. For the comparison of Ar–Ar ages among different samples from this study and with other Ar–Ar data, only the analytical errors are considered since the same uncertainties in the age of the flux monitor and decay constant apply to all samples equally and are important only when Ar–Ar results are compared with other dating methods. In Table 1, however, we report uncertainties in the weighted average ages using both the analytical errors alone and the total error that includes external factors. For all samples, the composition of ^{40}Ar/^{36}Ar$_{trapped}$ determined from the regression in the ^{36}Ar/^{40}Ar vs. ^{39}Ar/^{40}Ar diagram overlaps with atmospheric values within error.

Biotite from the Ombu granodiorite (sample 391) yielded a weighted average plateau age of 132.6 ± 1.0 Ma, which agrees within uncertainty with the isochron age using the same heating steps (Fig. 3). This age overlaps within the 2σ uncertainties with the U–Pb zircon date of 135.0 ± 1.6 (1σ) for the compositionally equivalent Ombu rhyodacite reported by Pirajno et al. (2000).

The biotite separates from two samples of the Erongo granite (454 and 212) did not yield statistically valid plateau ages. Their weighted average ages of 133.3 ± 1.1 and 133.1 ± 1.1 Ma are associated with high MSWD values (7.5 and 6.4, respectively). Nevertheless, the steps used for calculating the weighted average ages have Ca/K (^{37}Ar/^{39}Ar) and Cl/K (^{38}Ar/^{39}Ar) ratios that agree with the corresponding ratios measured by electron microprobe analysis (Fig. 4). Following Villa et al. (2000), agreement in these two sets of ratios implies that secondary alteration phases are insignificant and a reliable age for the biotite can be calculated.

The samples from the late-stage basic alkaline plugs (kaersutite and phlogopite from foidite

samples 435 and 432) yielded statistically indistinguishable plateau ages of 132.0 ± 1.0 and 130.8 ± 1.0 Ma, respectively. These ages agree with the geologic constraint that the alkaline plugs are the youngest magmatic units in the Erongo complex, and intrude the Ombu rhyodacite.

4.2. U–Pb ages

High-spatial resolution SIMS dating was applied to zircons from the Erongorus rhyodacite, Etuka rhyolite, Ombu granodiorite, and Erongo granite (Tables 2 and 3). Of all these units, the zircon grains from Erongorus rhyodacite are texturally and compositionally distinctive. They lack oscillatory zoning in CL images and commonly contain melt channels (Fig. 5). Compositionally, the Erongorus zircons have U contents (~ 3000 ppm) that exceed those of zircon from all the other units by about one order of magnitude and their Th/U ratios are also exceptionally high (average of 2.2 ± 0.4 compared to 0.5, 0.7, and 0.4 in Ombu granodiorite, Ekuta rhyolite, and Erongo granite, respectively). Another characteristic difference revealed in the age results is that the Erongorus rhyodacite appears to contain no pre-Mesozoic zircon grains (none of the 11 grains analyzed) whereas approximately 20–50% of the grains analyzed from the other units gave pre-Mesozoic ages. The sample coverage from each unit is small, however, so these observations are preliminary. For example, the Erongo granite sample 454 yielded only four useful grains.

U–Pb zircon ages for Erongorus rhyodacite cover a fairly wide range between 116 and 134 Ma (Fig. 6), and multiple analyses on individual grains revealed that some of this range is present locally, even within single grains (e.g. Fig. 5b,d). Zircon crystallization over almost 20 Ma is unlikely and the 116 Ma age is inconsistent with the stratigraphic position of the Erongorus rhyodacite below the Ombu unit, which is dated at about 135 Ma (Pirajno et al., 2000). We explain the younger ages as a result of a post-crystallization Pb-loss event whose age remains unresolved due to insufficient precision of the measurements. Note in Fig. 5d that the analyzed spot that

Table 2
U–Pb ion microprobe results for zircons from the Erongo complex, Namibia

Sample	U (ppm)	Th (ppm)	$^{206}Pb/^{238}U^a$	$^{206}Pb/^{238}U^a$ 1σ	$^{207}Pb/^{235}U^a$	$^{207}Pb/^{235}U^a$ 1σ	Error correlation	$^{207}Pb/^{206}Pb^a$	$^{207}Pb/^{206}Pb^a$ 1σ	Radiogenic ^{206}Pb (%)	Age^a (Ma) $^{206}Pb/^{238}U$	± Age^a (Ma) $^{206}Pb/^{238}U$	Age^a (Ma) $^{207}Pb/^{206}Pb$	± Age^a (Ma) $^{207}Pb/^{206}Pb$
Erongorus rhyodacite														
467_g3_1	3134	7187	0.0192	0.0004	0.117	0.006	0.63	0.0443	0.0020	98.3	122.4	2.5	–	–
467_g4_1	2185	4653	0.0207	0.0004	0.137	0.006	0.66	0.0480	0.0016	99.0	132.1	2.4	97.2	79.8
467_g5_1	1559	3362	0.0195	0.0003	0.125	0.008	0.39	0.0466	0.0029	98.6	124.6	2.2	29.5	150.0
467_g6_1	2186	6554	0.0204	0.0003	0.129	0.011	0.46	0.0459	0.0034	97.0	130.4	2.2	–	–
467_g7_1	2920	5196	0.0209	0.0004	0.136	0.004	0.78	0.0473	0.0009	99.5	133.3	2.7	65.4	46.2
467_g8_1	3483	8478	0.0182	0.0004	0.131	0.010	0.30	0.0523	0.0039	92.0	116.0	2.5	297.5	171.0
467_g10_1	2335	7059	0.0189	0.0003	0.127	0.008	0.63	0.0487	0.0025	99.0	120.5	2.2	130.9	118.0
467_g11_1	3108	6671	0.0194	0.0003	0.130	0.006	0.32	0.0486	0.0021	98.8	123.9	2.0	127.8	99.2
467_g12_1	1766	3063	0.0187	0.0003	0.131	0.011	0.65	0.0506	0.0036	98.6	119.4	2.0	224.1	164.0
467_g14_1	2436	6059	0.0210	0.0004	0.138	0.006	0.41	0.0475	0.0020	99.1	133.9	2.3	76.3	102.0
E467_g7_2	6280	3892	0.0202	0.0004	0.132	0.028	0.58	0.0474	0.0095	96.3	129.2	2.8	67.2	478.0
E467_g8_2	7535	3966	0.0193	0.0004	0.122	0.024	0.56	0.0459	0.0084	94.6	122.9	2.6	–	–
E467_g14_2	4274	2076	0.0182	0.0005	0.149	0.029	0.54	0.0592	0.0106	96.0	116.3	2.9	576.1	390.0
Ekuta rhyolite														
469_g2_1	227	163	0.0208	0.0011	0.154	0.044	0.40	0.0535	0.0144	92.9	132.9	6.7	348.0	608.0
469_g4_1	227	100	0.0225	0.0008	0.185	0.049	0.38	0.0594	0.0151	94.6	143.6	5.3	582.5	551.0
469_g6_1	–	–	0.0765	0.0032	0.589	0.058	0.57	0.0559	0.0046	97.4	475.0	18.9	447.8	184.0
469_g8_1	209	274	0.0226	0.0009	0.134	0.047	0.49	0.0431	0.0142	93.2	144.0	5.8	–	–
469_g9_1	–	–	0.0593	0.0016	0.474	0.041	0.54	0.0580	0.0044	97.4	371.2	9.5	528.3	165.0
469_g11_1	–	–	0.1580	0.0078	1.600	0.091	0.96	0.0736	0.0013	99.2	944.7	43.4	1030.0	35.1
469_g12_1	198	144	0.0200	0.0011	0.120	0.060	0.44	0.0434	0.0207	88.8	127.8	7.2	–	–
469_g13_1	140	103	0.0182	0.0013	0.096	0.078	0.48	0.0381	0.0297	85.6	116.4	7.9	–	–
469_g15_1	376	176	0.0186	0.0010	0.101	0.056	0.48	0.0396	0.0210	89.9	118.5	6.5	–	–
469_g15_2	229	93	0.0201	0.0012	0.108	0.064	0.44	0.0388	0.0223	88.8	128.3	7.4	–	–

[a] After common Pb-correction using $^{206}Pb/^{204}Pb = 18.9$ and $^{207}Pb/^{204}Pb = 15.6$.

Table 3
U–Pb ion microprobe results for zircons from the Erongo complex, Namibia

Sample	U (ppm)	Th (ppm)	$^{206}Pb/^{238}U^a$	$^{206}Pb/^{238}U^a$ 1σ	$^{207}Pb/^{235}U^a$	$^{207}Pb/^{235}U^a$ 1σ	Error correlation	$^{207}Pb/^{206}Pb^a$	$^{207}Pb/^{206}Pb^a$ 1σ	Radiogenic ^{206}Pb (%)	Age^a (Ma) $^{206}Pb/^{238}U$	± Age^a (Ma) $^{206}Pb/^{238}U$	Age^a (Ma) $^{207}Pb/^{206}Pb$	± Age^a (Ma) $^{207}Pb/^{206}Pb$
Erongo granite														
E454_g3_s1	263	80	0.0211	0.0007	0.117	0.041	0.55	0.0404	0.0133	96.0	134.3	4.3	–	–
454_g3_2	–	–	0.0211	0.0008	0.129	0.041	0.44	0.0446	0.0134	94.0	134.3	5.1	–	–
454_g3_3	–	–	0.0202	0.0006	0.167	0.045	0.40	0.0599	0.0154	94.7	129.1	3.8	600.6	557.0
454_g4_s1	634	85	0.0202	0.0004	0.134	0.008	0.41	0.0480	0.0028	98.8	129.0	2.8	99.1	136.0
E454_g7_s1	–	–	0.0722	0.0012	0.575	0.011	0.82	0.0577	0.0006	99.8	449.3	7.4	519.6	24.1
454_g7_2	–	–	0.0500	0.0009	0.406	0.008	0.76	0.0589	0.0008	98.4	314.4	5.5	562.5	27.8
E454_g15_s1	302	138	0.0198	0.0005	0.123	0.040	0.59	0.0451	0.0139	95.4	126.4	3.3	–	–
E454_g15_s2	366	187	0.0207	0.0006	0.128	0.028	0.48	0.0447	0.0093	95.6	132.1	3.6	–	–
454_g15_3	310	126	0.0213	0.0011	0.164	0.040	0.48	0.0560	0.0127	96.1	135.5	6.9	453.1	502.0
Ombu granodiorite														
E460_g1_s1	409	154	0.0202	0.0004	0.144	0.016	0.55	0.0517	0.0054	98.6	128.7	2.7	269.8	238.0
E460_g2_s1	303	165	0.0227	0.0006	0.161	0.033	0.53	0.0513	0.0100	97.5	144.8	4.0	255.0	447.0
E460_g3_s1	–	–	0.0902	0.0020	0.719	0.025	0.75	0.0578	0.0014	99.6	556.5	11.6	522.3	51.1
E460_g5_s1	437	223	0.0225	0.0005	0.164	0.020	0.44	0.0529	0.0060	97.9	143.3	3.3	325.1	256.0
E460_g6_s1	–	–	0.0931	0.0026	0.758	0.025	0.82	0.0591	0.0011	99.3	573.8	15.3	569.8	41.5
E460_g7_s1	230	57	0.0212	0.0006	0.158	0.033	0.53	0.0540	0.0106	96.6	135.3	3.9	372.1	441.0
460_g8_1	200	89	0.0201	0.0012	0.116	0.049	0.49	0.0418	0.0166	93.0	128.0	7.3	–	–
460_g9_1	242	105	0.0217	0.0009	0.175	0.044	0.52	0.0584	0.0136	93.6	138.5	5.6	546.1	510.0
460_g10_1	249	124	0.0230	0.0009	0.161	0.059	0.35	0.0506	0.0179	91.7	146.8	5.9	222.0	820.0
460_g11_1	263	115	0.0224	0.0012	0.151	0.037	0.44	0.0488	0.0110	94.7	142.7	7.2	139.3	531.0
460_g12_1	442	279	0.0232	0.0010	0.134	0.032	0.44	0.0418	0.0095	95.2	147.7	6.0	–	–

^{a} After common Pb-correction using $^{206}Pb/^{204}Pb = 18.6$ and $^{207}Pb/^{204}Pb = 15.6$.
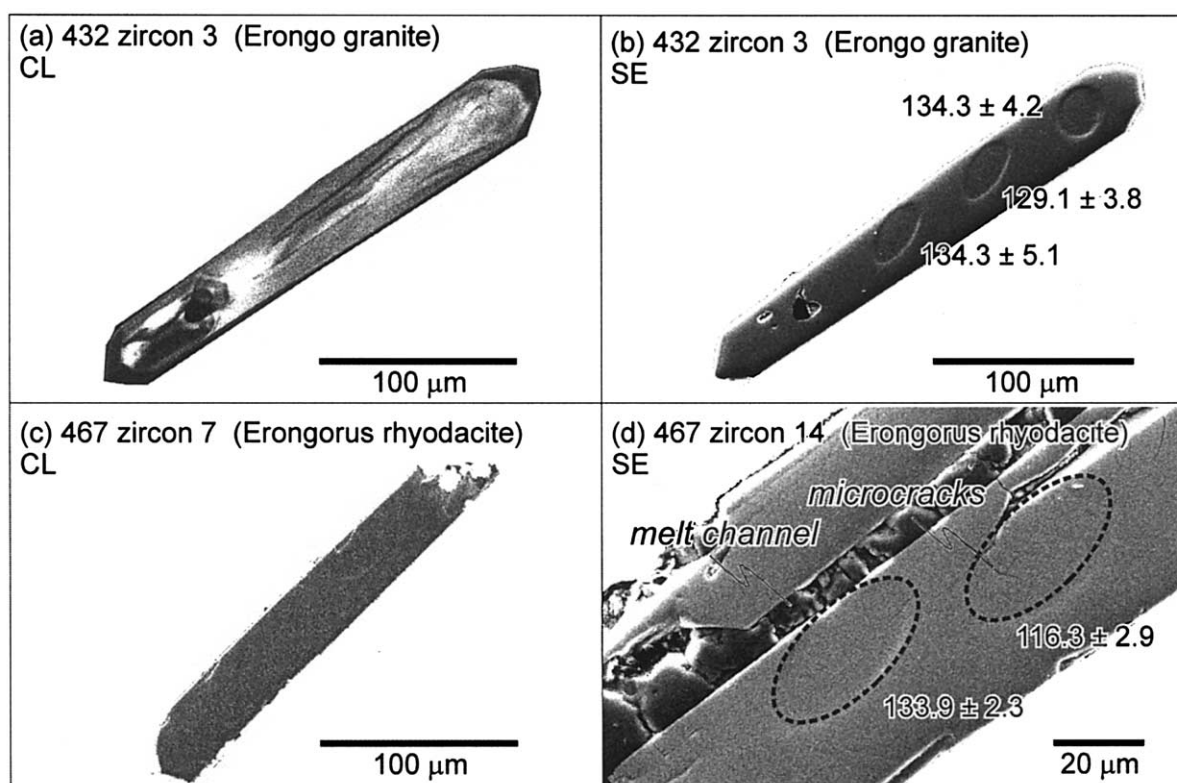
Fig. 5. Cathodoluminescense (CL) and secondary electron (SE) images of Erongo zircons. (a,b) Erongo granite; (c,d) Erongorus rhyodacite. Note the lack of CL visible oscillatory zoning in (c) and beam overlap with microcrack for the 116 Ma spot in (d).

yielded an apparent 116 Ma age overlaps with a microcrack, whereas an adjacent spot on the undamaged portion of the grain yielded an older age (~ 134 Ma) which agrees with other grains of the same unit and is consistent with field relationships. Such microcracks are common in Erongorus zircons and could have provided access for fluids leaching radiogenic Pb. We consequently excluded the younger ages obviously affected by Pb-loss and calculated a weighted mean age from the remaining analyses. We limited the analyses used for calculating the weighted mean age by using the MSWD criterion (within 95% confidence boundaries; Mahon, 1996) to distinguish zircon analyses representing a single population in which variations are due to analytical scatter only. By excluding younger ages, we obtained 131.8 ± 1.0 Ma (MSWD = 0.6; number of analyses $n = 5$) as our best estimate for the age of zircon crystallization in the Erongorus rhyodacite. Two

of 11 analyzed zircons from the Ombu granodiorite yielded clearly Pre-Mesozoic ages of ~ 560 Ma. The weighted average age of the remaining analyses (137.7 ± 2.5; MSWD = 3.2; $n = 9$) is indistinguishable from the weighted average of zircon ages (137.2 ± 2.6; MSWD = 7.6; $n = 12$) reported for the volcanic equivalent of the granodiorite by Pirajno et al. (2000). Pirajno et al. (2000) noted the problem of inherited zircons in this unit and proposed a best estimate for the emplacement age of 135.0 ± 1.6 Ma by excluding two older ages (150 and 175 Ma) that were interpreted as mixed ages resulting from partial primary ion beam overlap with older parts of the grains. If we follow the same reasoning and exclude analyses giving geologically unsupported intermediate ages, we obtain a preferred weighted mean age for zircon crystallization in the Ombu granodiorite magma of 132.3 ± 1.9 Ma (MSWD = 1.5; $n = 5$). U–Pb zircon ages for the Erongo
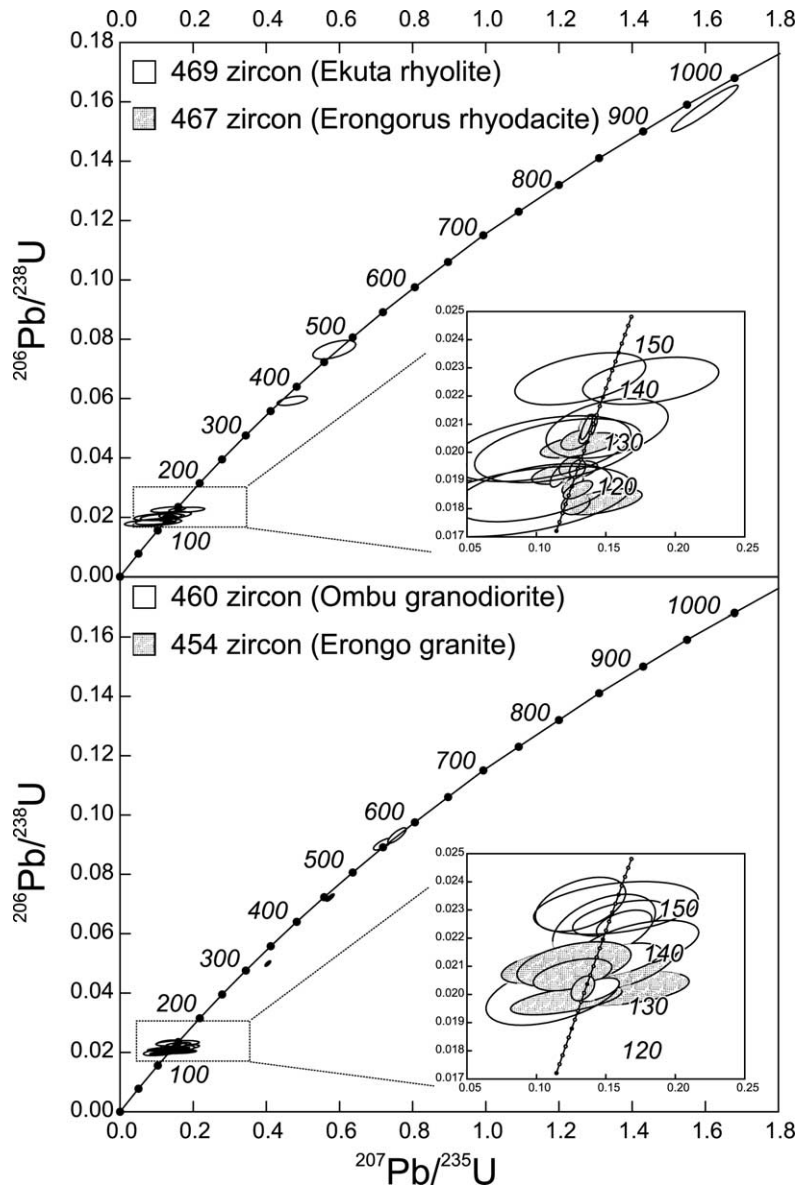
Fig. 6. ^{206}Pb/^{238}U vs. ^{207}Pb/^{235}U concordia diagrams for volcanic and plutonic samples of the Erongo complex.

granite and the compositionally equivalent Ekuta rhyolite overlap within uncertainty (130.3 ± 1.4; MSWD = 0.7 and 132.6 ± 4.2; MSWD = 3.0, respectively). The high MSWD of the latter suggests additional non-analytical scatter that could be caused by Pb-loss and/or inheritance of older zircon not seen in CL images. Both units also contain abundant pre-Mesozoic zircons although, un-

like the Ombu rhyodacite and granodiorite, the rocks lack any visible lithic fragments.

Most of the concordant pre-Mesozoic zircon ages from our results cluster between 550 and 600 Ma, which corresponds closely with the age range of Damara granites in the vicinity of Erongo (e.g. Jung et al., 2000). The few clearly discordant analyses, which are attributed to either beam
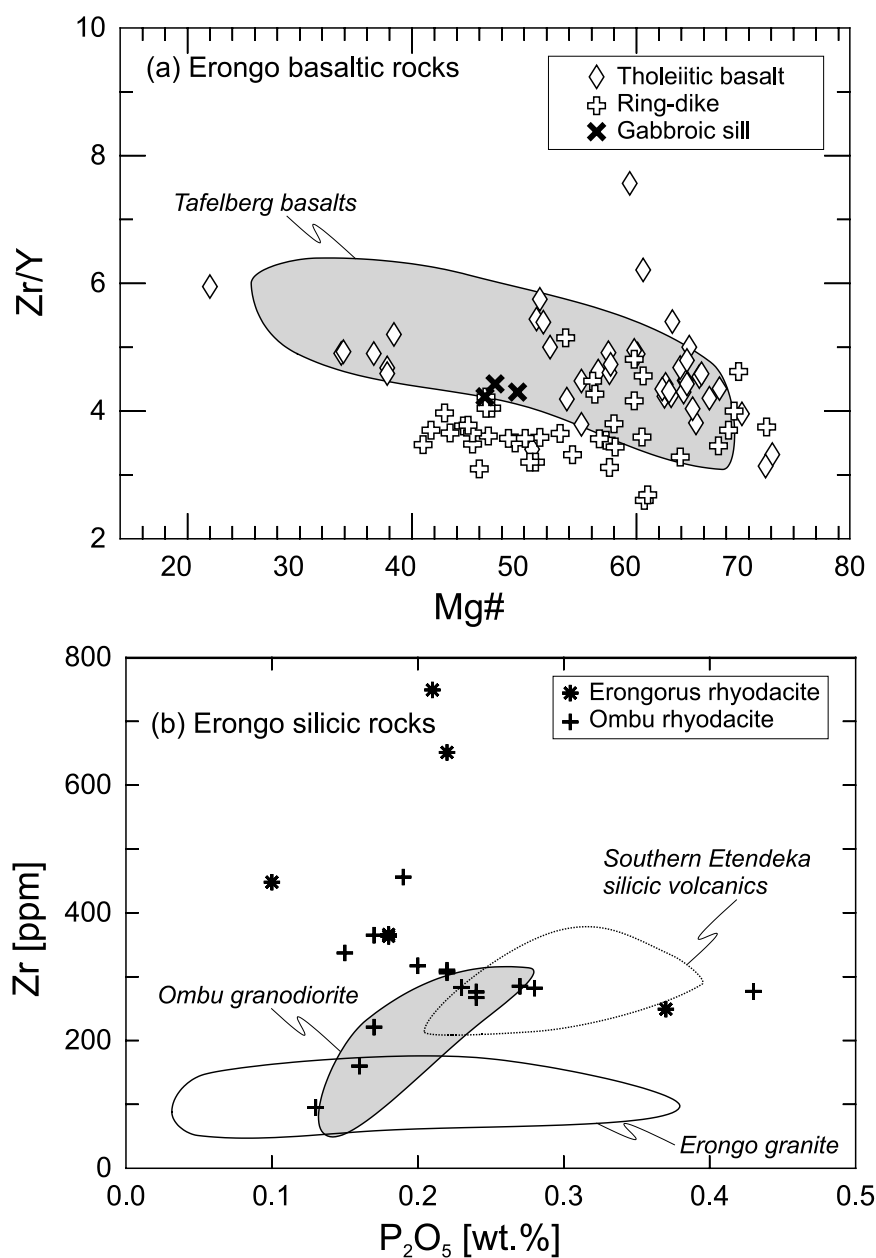
Fig. 7. Compositional comparison of Erongo intrusive and extrusive units (authors' unpublished data) with regional volcanic rocks of the Etendeka province: (a) comparison between basal tholeiitic basalts, ring dike and gabbroic sill with a field for Tafel-berg basalts from Marsh et al. (2001). (b) comparison between silicic units of the Erongo complex with a field for southern Eten-deka silicic volcanic rocks from Ewart et al. (1998) and Marsh et al. (2001). Note the limited overlap in composition between Erongo units and southern Etendeka silicic volcanic rocks (see also Table 4).

Table 4
Comparison of trace element ratios between silicic units of the Erongo complex and southern Etendeka volcanic units

	Nb/Ta	Th/Yb	Ta/Yb	(La/Yb)$_{CN}$	Zr/Nb	Ti/Sm	Ti/Zr
Erongo complex[a]							
Erongorus rhyodacite	9.9–20	4.4–5.3	0.21–0.23	0.8–10.6	10.4–33.3	203–316	5.2–23.9
Ombu rhyodacite	11.6–17.5	5.5–6.5	0.29–0.33	0.4–10.1	8.3–33.7	416–479	6.8–21.2
Ombu granodiorite	12.9–17.5	5.0–6.4	0.31–0.43	0.4–9.9	8.1–24.3	300–531	11.5–23.4
Southern Etendeka[b]							
Goboboseb rhyodacite	9.2–11.1	3.0–4.0	0.47–0.59	0.0–7.9	11.9–13.6	664–711	19.5–21.0
Springbok rhyodacite	9.2–9.6	3.5–4.0	0.58–0.63	0.7–8.0	11.3–13.0	664–672	19.6–21.3

[a] Values represent the range from authors' unpublished data.
[b] Values represent the range of samples reported by Ewart et al. (1998), who used the term quartz latite.

overlap with younger parts of the grains or post-crystallization Pb-loss, also yield Cambrian ^{207}Pb/^{206}Pb ages (560 ± 30 and 520 ± 24 Ma). Similar ages of pre-Mesozoic zircon from the Ombu rhyodacite were reported by Pirajno et al. (2000), although we have found no ages > 1000 Ma. We concur with their interpretation that these zircons represent basement xenocrysts and they are not considered further in this report.

5. Discussion

5.1. Volcanic stratigraphy and relations to the Etendeka Group

Despite the excellent exposures of the volcanic sequence preserved along the margins of the Erongo complex (Fig. 2), it is difficult to determine the relationship of Erongo units with the regional Etendeka sequence since the nearest outcrops of the latter are more than 100 km to the northwest in the Goboboseb mountains around Messum (Fig. 1). Emmermann (1979) and Pirajno (1990) both suggested that the basal basaltic lavas belong to the regional flood basalts and new analytical data demonstrate their close similarity in trace element and isotopic composition (authors' unpublished data). One of the distinctive characteristics of the Etendeka sequence in the Goboboseb region is the abundance of rhyodacite units upward in the sequence, and this raises the question whether the basal rhyodacite (Erongorus unit), which overlies basalt at Erongo, also correlates with similar rocks of the Etendeka Group.

The upper (Ombu) rhyodacite has an intrusive equivalent exposed in the deeper interior of the central massif and it is clearly locally derived, but there is some evidence that the Erongorus rhyodacite is not. One point is the uneven distribution of Erongorus tuff, which is found only on the western margin of the complex whereas in the east, the Ombu unit overlies basalt. Second, the Erongorus unit lacks lithic fragments and inherited zircons whereas both of these features are characteristic of the volcanic and intrusive facies of the Ombu magma. Finally, our U–Pb zircon ages for the Erongorus unit agree closely with ages from the Etendeka silicic volcanics in NW Namibia (Fig. 8) although it must be said that the U–Pb ages of the Ombu granodiorite and Erongo granite also overlap. The radiometric age data are permissive but not conclusive evidence for a relationship of the basal Erongo units with the Etendeka sequence. Additional arguments can be made from geochemical comparisons based on the overview of compositional groups in the Etendeka volcanic sequences from Namibia by Marsh et al. (2001) and further data from Ewart et al. (1998). Using the incompatible trace element ratios that were found to best discriminate the Etendeka basalt types (e.g. Zr/Y; Fig. 7a), we find a good correlation between the basal Erongo tholeiitic basalts and the volumetrically dominant Tafelberg-type basalts of the Etendeka province. While this observation also holds for the gabbroic sill, most of the Erongo ring-dike samples plot at lower Zr/Y values for a given Mg# compared to Tafelberg-type basalts (Fig. 7a).
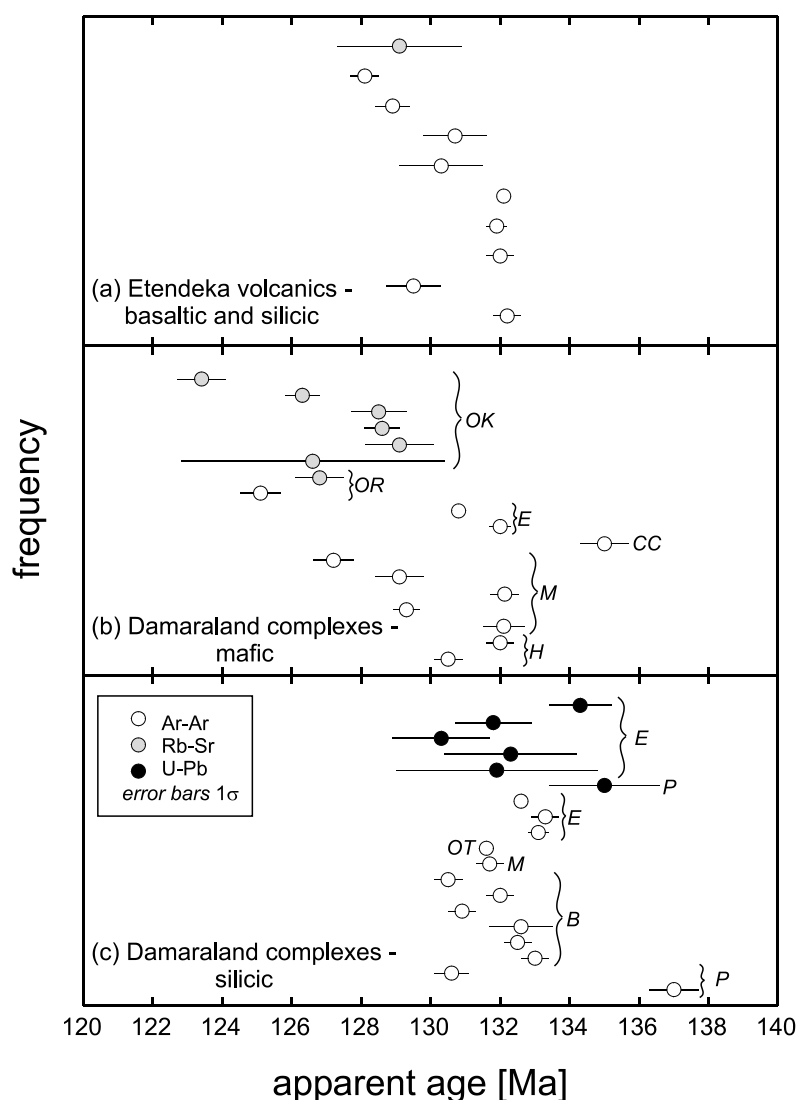
Fig. 8. Summary of radiometric age dating results for the Etendeka province. Data sources for volcanic rocks: Milner et al., 1995, Renne et al., 1996, Kirstein et al., 2001. Abbreviation and data sources for the Damaraland complexes: B: Brandberg (Schmitt et al., 2000); CC: Cape Cross (Milner et al., 1995); E: Erongo (Pirajno et al., 2000); H: Huab sills (Milner et al., 1993); M: Messum (Renne et al., 1996); OK: Okenyenya (Milner et al., 1993); OR: Okurusu (Milner et al., 1995); OT: Otjo-horongo (Pirajno et al., 2000); P: Paresis (Milner et al., 1995; Pirajno et al., 2000). Note: contact relations commonly indicate that Damaraland intrusives (lower panels) post-date volcanic activity (upper panel), and the 137 Ma age of Paresis comendite (Milner et al., 1995) is stratigraphically inconsistent with the 131 Ma age for Paresis quartz–feldspar porphyry reported by Piraj-no et al. (2000).

For the silicic units, comparisons of selected trace element ratios are given in Table 4 and Fig. 7b. One point to emphasize is the compositional similarity between the Ombu rhyodacite and granodiorite (Emmermann, 1979). Second, although there is some overlap between the Ombu and Erongorus samples, the Erongorus rhyodacite has distinctly lower ratios of Th/Yb, Ta/Yb and Ti/Sm, and ranges to much higher Zr than the Ombu units. The two units also

have different Sr- and Nd-isotopic composition (authors' unpublished data), and contrasting U–Th concentration and abundance ratios in zircons (Table 2). Finally, the Erongorus and Ombu rhyodacites are petrographically distinct (scarcity of lithic fragments and absence of xenocrystic zircons in Erongorus versus their abundance in the Ombu rocks) and only the Ombu rhyodacite has an intrusive equivalent within the Erongo complex (Ombu granodiorite). We tentatively conclude therefore that the Erongorus unit erupted from an external source. The identity of this source is uncertain but geochemical data suggest that the Erongorus rhyodacite is not equivalent to the regional silicic volcanic units. On the one hand, the rhyodacite shows a much greater compositional variability than the Etendeka volcanic rocks, and there are also significant differences in trace element ratios (especially Ti/Sm, Th/Yb, Ta/Yb, see Table 4) and Zr–P_2O_5 concentrations (Fig. 7b). The silicic magmas unambiguously linked to the Erongo complex as a source are the geochemical twins Ombu rhyodacite–Ombu granodiorite and Ekuta rhyolite–Erongo granite (Fig. 7b).

5.2. Timing of silicic magmatism in the Damaraland complexes

Our geochronological results indicate a relatively short duration for the emplacement of silicic magmas at the Erongo complex. Furthermore, the overlap in age between the Ombu rhyodacite and Erongo granites with alkaline basic magmas that intrude them argue against a long-lived zone of partial melting below the complex. This is because layers of silicic partial melts within the crust will act as density barriers for the ascent of basic magma, thus impeding the ascent and facilitating crustal contamination of the latter. The basic alkaline rocks from Erongo erupted quickly as witnessed by their diatreme structures and they show little or no crustal contamination (Trumbull et al., 2003); thus it is unlikely that a zone of felsic melts existed below the complex at the time of their emplacement.

To further compare our results with the regional geochronologic pattern for the Damaraland

complexes and the regional Etendeka volcanic sequence as a whole we have compiled age data from all recent geochronologic studies that reported $^{40}Ar/^{39}Ar$, high spatial resolution U–Pb zircon, or Rb–Sr mineral isochron ages (Fig. 8). Our interest is on reasonably precise and reliable ages and therefore we chose not to include K–Ar data because Milner et al. (1995) showed that K–Ar ages from this province yield a broader range than other methods and attributed the difference to Ar-loss in some cases and the presence of excess radiogenic Ar in others. A good example of Ar-loss is the discrepancy between K–Ar and $^{40}Ar/^{39}Ar$ step-heating ages of biotite from the Brandberg granite. Watkins et al. (1994) reported K–Ar biotite ages as young as 125 Ma whereas the $^{40}Ar/^{39}Ar$ step-heating results from Schmitt et al. (2000) showed a plateau age of ∼133 ± 2 Ma and younger apparent ages for the initial Ar release steps, which indicate post-crystallization Ar-loss. We also do not include results from Rb–Sr whole-rock isochron ages because initial heterogeneity of $^{87}Sr/^{86}Sr$ is likely in these composite complexes and it has been previously recognized (e.g. Milner et al., 1993).

Comparison of age distribution of the Etendeka volcanic rocks and silicic units in the Damaraland complexes demonstrates very similar peak ages and age ranges (Fig. 8a,c). The basic units from the complexes also show 132 Ma ages (Messum, Huab sills, Erongo) but the age distribution for the basic units appears to be skewed to younger values, suggesting a longer duration of basic magmatism, to as young as 123 Ma (Milner et al., 1993). The ages of felsic subvolcanic complexes Erongo, Brandberg, and Paresis indicate coeval activity over distances of up to 150 km, and this corroborates previous findings that activity along Damaraland magmatic lineaments (e.g. Cape Cross–Okurusu) was broadly contemporaneous and shows no age progression inland (Milner et al., 1995).

We suggest that the smaller age range of silicic units from the Damaraland complexes compared with the basic rocks is related to the petrogenesis of the magmas. It has been shown that the silicic magmas are partly or dominantly derived from crustal melting (Harris, 1995; Mingram et al.,

2000; Schmitt et al., 2000; Trumbull et al., 2000) and the coincidence in age distribution between the silicic units and the Etendeka flood basalts suggests that this crustal melting and/or assimilation took place in a single event related to heat from the extensive basaltic magmas. Thereafter, basaltic magma continued to be generated but at much smaller volumes than in the flood-basalt event, whereas the fusible portions of the crust may have been exhausted, particularly since the Damara crust had already been heavily involved in partial melting to produce granites in the early Cambrian (Jung et al., 2000). Thus, silicic magmatism in the Damaraland complexes appears to have been short-lived and ceased by about $\sim$130 Ma. However, it is interesting that silicic volcanism in southern Uruguay apparently persisted until at least $\sim$127 Ma (Kirstein et al., 2001), significantly younger than the main flood-basalt event in the Paraná province, whose peak was contemporaneous with the Etendeka eruptions. The more protracted silicic magmatism in the southern Paraná province could be related to additional heat input by mantle melting near the margins of the opening South Atlantic, whereas further inland in the Damaraland area, decompression melting was less efficient in the mantle underlying a thicker lithospheric lid.

6. Summary and conclusions

$^{40}Ar/^{39}Ar$ and U–Pb zircon dating of intrusive and extrusive rocks from the Erongo complex, Namibia, provides insights into the duration of bimodal magmatism within a single composite volcanic center. The early erupted tholeiitic basalts and the overlying Erongorus rhyodacite have no intrusive equivalents within the Erongo complex. They are likely to represent lavas and tuffs erupted from an unknown external source. Whereas the tholeiitic basalts closely resemble the dominant Tafelberg basalts of the southern Etendeka province, the rhyodacite is compositionally distinct from the southern Etendeka silicic volcanic rocks. Silicic units higher up in the stratigraphic sequence (Ombu rhyodacite and Ekuta rhyolite) are clearly related to the Erongo intru-

sive rocks (Ombu granodiorite and Erongo granite, respectively) and were therefore locally derived. $^{40}Ar/^{39}Ar$ and U–Pb ages for the silicic units overlap within error when analytical, decay constant and flux monitor uncertainties are taken into account. The youngest ages were obtained for phlogopite from a foiditic intrusion ($\sim$130.8 ± 1.0 Ma) within Ombu rhyodacite. Compositionally similar alkali basaltic dikes also intrude the Erongo granite.

This study has shown that the age of extrusive and intrusive activity at Erongo overlaps with the peak episode of flood-basalt effusion in the Etendeka–Paraná province. We conclude that:

(1) Silicic magmatism at Erongo had a maximum duration of only a few million years and probably less than 2 Ma.

(2) Erongo silicic magmas formed during a single crustal heating pulse at the height of flood-basalt effusion.

(3) Silicic magmatism with variable but significant crustal contributions (Trumbull et al., 2000) occurred simultaneously in the Damaraland complexes at the time of Etendeka flood volcanism and ceased at about 130 Ma, when heating of the crust by the extensive mantle melting waned. Basic magmatism in the Damaraland complexes continued sporadically and at lower volumes to about 123 Ma, but lacked the power to create further crustal melting.

notes on Erongo geology. Reviews by S. Jung und J.S. Marsh helped improve the quality of the manuscript.

References

Bryan, S.E., Riley, T.R., Jerram, D.A., Stephens, C.J., Leat, P.T., 2002. Silicic volcanism: an undervalued component of large igneous provinces and volcanic rifted margins. Geol. Soc. Am. Spec. Pap. 362, 97–118.

Cloos, H., 1911. Geologische Beobachtungen in Südafrika II. Geologie des Erongo im Hererolande. Beiträge zur geologischen Erforschung der deutschen Schutzgebiete 3, 84 pp.

Cloos, H., 1919. Der Erongo: ein vulkanisches Massif im Tafelgebirge des Hererolandes und seine Bedeutung für die Raumfrage plutonischer Massen. Beiträge zur geologischen Erforschung der deutschen Schutzgebiete 17, 233 pp.

Compston, W., Williams, I.S., Meyer, C., 1984. U–Pb geochronology of zircons from lunar breccia 73217 using a sensitive high mass-resolution ion microprobe. J. Geophys. Res. Suppl. 89, B525–B534.

Emmermann, R., 1979. Aufbau und Entstehung des Erongo-Komplexes. In: W.D. Blümel, R. Emmermann, K. Hüser (Eds.), Der Erongo. Geowissenschaftliche Beschreibung und Deutung eines südwestafrikanischen Vulkankomplexes. Southwest African Scientific Society, Windhoek, pp. 16–53.

Erlank, A.J., Marsh, J.S., Duncan, A.R., Miller, R.M., Hawkesworth, C.J., Betton, P.J., Rex, D.C., 1984. Geochemistry and petrogenesis of the Etendeka volcanic rocks from SWA/Namibia. In: A.J. Erlank (Ed.), Spec. Publ. Geological Society of South Africa 13, pp. 195–246.

Ewart, A., Milner, S.C., Armstrong, R.A., Duncan, A.R., 1998. Etendeka volcanism of the Goboseb Mountains and Messum Igneous Complex, Namibia. Part II: voluminous quartz latite volcanism of the Awahab magma system. J. Petrol. 39, 227–253.

Ewart, A., Milner, S.C., Duncan, A.R., Bailey, M., 2002. The Cretaceous Messum igneous complex, S.W. Etendeka, Namibia; reinterpretation in terms of a downsag-cauldron subsidence model. J. Volcanol. Geotherm. Res. 114, 251–273.

Harris, C., 1995. Oxygen isotope geochemistry of the Mesozoic anorogenic complexes of Damaraland, Northwest Namibia; evidence for crustal contamination and its effect on silica saturation. Contrib. Mineral. Petrol. 122, 308–321.

Harris, C., Marsh, J.S., Milner, S.C., 1999. Petrology of the alkaline core of the Messum igneous complex: evidence for progressively decreasing effect of crustal contamination. J. Petrol. 40, 1377–1397.

Hegenberger, W., 1988. Karoo sediments of the Erongo mountains, their environmental setting and correlation. Commun. Geol. Surv. Southwest Africa/Namibia 4, 51–57.

Jung, S., Hoernes, S., Mezger, K., 2000. Geochronology and petrogenesis of Pan-African, syn-tectonic, S-type and post-tectonic A-type granite (Namibia): products of melting of crustal sources, fractional crystallization and wallrock entrainment. Lithos 50, 259–287.

Kirstein, L.A., Kelley, S., Hawkesworth, C., Turner, S., Mantovani, M., Wijbrans, J., 2001. Protracted felsic magmatic activity associated with the opening of the South Atlantic. J. Geol. Soc. Lond. 158, 583–592.

Mahon, K., 1996. The New 'York' regression: application of an improved statistical method to geochemistry. Int. Geol. Rev. 38, 293–303.

Martinez, I.A., Harris, C., LeRoex, A.P., Milner, S.C., 1996. Oxygen isotope evidene for extensive crustal contamination in the Okenyenya complex, Namibia. Geochim. Cosmochim. Acta 60, 4497–4508.

Marsh, J.S., Ewart, A., Milner, S.C., Duncan, A.R., Miller, R.M., 2001. The Etendeka igneous province: magma types and their stratigraphic distribution with implications for the evolution of the Paraná-Etendeka flood basalt province. Bull. Volcanol. 62, 464–486.

McNeill, G.W., 1989. A geochemical study of three Namibian igneous complexes. M.Sc. Thesis, University of St. Andrews, Department of Geology, 57 pp.

Martin, H., Mathias, M., Simpson, E.S.W., 1960. The Damaraland sub-volcanic ring complexes in South West Africa. Report of the International Geological Congress XXI Session 13, pp. 156–174.

Miller, R.M., 1983. The Pan-African Damara orogen of South West Africa/Namibia. In: R.M. Miller (Ed.), Spec. Publ. Geological Society of South Africa 11, pp. 431–515.

Milner, S.C., Le Roex, A.P., 1996. Isotope characteristics of the Okenyenya igneous complex, Northwestern Namibia: Constraints on the composition of the early Tristan plume and the origin of the EM 1 mantle component. Earth Planet. Sci. Lett. 141, 277–291.

Milner, S.C., Le Roex, A., Watkins, R.T., 1993. Rb-Sr determination of rocks from the Okenyenya igneous complex, northwestern Namibia. Geol. Mag. 130, 335–343.

Milner, S.C., Le Roex, A.P., O'Connor, J.M., 1995. Age of Mesozoic igneous rocks in northwestern Namibia, and their relationship to continental breakup. J. Geol. Soc. Lond. 152, 97–104.

Milner, S.C. (Ed.), 1997. Geological map of Namibia (1:250,000). Sheet 2114-Omaruru. Geological Survey of Namibia.

Mingram, B., Trumbull, R.B., Littmann, S., Gerstenberger, H., 2000. A petrogenetic study of anorogenic felsic magmatism in the Cretaceous Paresis ring complex, Namibia: evidence for crust-mantle hybridization. Lithos 54, 1–22.

Onstott, T.C., Miller, M.L., Ewing, R.C., Arnold, G.W., Walsh, D.S., 1995. Recoil refinements; implications for the $^{40}Ar/^{39}Ar$ dating technique. Geochim. Cosmochim. Acta 59, 1821–1834.

Paces, J.B., Miller, J.D., 1993. Precise U–Pb ages of Duluth Complex and related mafic intrusions, northeastern Minnesota; geochronological insights to physical, petrogenetic, paleomagnetic, and tectonomagnetic processes associated with the 1.1 Ga Midcontinent Rift System. J. Geophys. Res. 98, 13997–14013.

Peate, D.W., 1997. The Paraná - Etendeka Province. In: J.J. Mahoney, M.F. Coffin (Eds.), Large Igneous Provinces, Geophys. Monogr. 100. American Geophysical Union, Washington, DC, pp. 217–246.

Pirajno, F., Phillips, D., Armstrong, R.A., 2000. Volcanology and eruptive history of the Erongo Volcanic Complex and the Paresis Igneous Complex: implications for mineral deposit styles. Commun. Geol. Surv. Namibia 12, 301–312.

Pirajno, F., 1990. The geology, geochemistry and mineralization of the Erongo Volcanic Complex, Namibia. South African J. Geol. 93, 485–504.

Pouchou, J.L., Pichoir, F., 1984. Un nouveau modèle de calcul pour la microanalyse quantitative par spectrométrie de rayons X. Rech. Aérosp. 3, 167–192.

Renne, P.R., Ernesto, M., Pacca, I.G., Coe, R.S., Glen, J.M., Prevot, M., Perrin, M., 1992. The age of Paraná flood volcanism, rifting of Gondwanaland, and the Jurassic-Cretaceous boundary. Science 258, 975–979.

Renne, P.R., Glen, J.M., Milner, S.C., Duncan, A.R., 1996. Age of Etendeka flood volcanism and associated intrusions in southwestern Africa. Geology 24, 659–662.

Renne, P.R., Swisher, C.C., Deino, A.L., Karner, D.B., Owens, T.L., DePaolo, D.J., 1998. Intercalibration of standards, absolute ages and uncertainties in $^{40}Ar/^{39}Ar$ dating. Chem. Geol. 145, 117–152.

Samson, S.D., Alexander, E.C., Jr., 1987. Calibration of the interlaboratory $^{40}Ar/^{39}Ar$ dating standard, MMhb-1. Chem. Geol. 66, 27–34.

Sañudo-Wilhelmy, S.A., Flegal, A.R., 1994. Temporal variations in lead concentrations and isotopic composition in the Southern California Bight. Geochim. Cosmochim. Acta 58, 3315–3320.

Schmitt, A.K., Emmermann, R., Trumbull, R.B., Bühn, B., Henjes-Kunst, F., 2000. Petrogenesis and $^{40}Ar/^{39}Ar$ geochronology of the Brandberg Complex, Namibia: evidence for a major mantle contribution in metaluminous and peralkaline granites. J. Petrol. 41, 1207–1239.

Stewart, K., Turner, S., Kelley, S., Hawkesworth, C.J., Kirstein, L., Mantovani, M., 1996. 3-D, $^{40}Ar-^{39}Ar$ Geochronology in the Paraná continental flood basalt province. Earth Planet. Sci. Lett. 143, 95–109.

Trumbull, R.B., Emmermann, R., Bühn, B., Gerstenberger, H., Mingram, B., Schmitt, A., Volker, F., 2000. Insights on the genesis of the Cretaceous Damarland igneous complexes in Namibia from a Nd- and Sr-isotopic perspective. Commun. Geol. Surv. Namibia 12, 313–324.

Trumbull, R.B., Bühn, B., Romer, R.L., Volker, F., 2003. The petrology of basanite-tephrite intrusions in the Erongo complex and implications for a plume origin of Cretaceous alkaline complexes in Namibia. J. Petrol. 44, 93–111.

Villa, I.M., Hermann, J., Müntener, O., Trommsdorf, V., 2000. $^{39}Ar-^{40}Ar$ dating of multiply zoned amphibole generations (malenco, Italian Alps). Contrib. Mineral. Petrol. 140, 363–381.

Watkins, R.T., McDougall, I., Le Roex, A.P., 1994. K-Ar ages of the Brandberg and the Okenyenya igneous complexes, north-western Namibia. Geol. Rundsch. 83, 348–356.

Wiedenbeck, M., Alle, P., Corfu, F., Griffin, W.L., Meier, M., Oberli, F., Von Quadt, A., Roddick, J.C., Spiegel, W., 1995. Three natural zircon standards for U-Th-Pb, Lu-Hf, trace element and REE analyses. Geostand. Newsl. 91, 1–23.